



저작자표시-비영리-변경금지 2.0 대한민국

이용자는 아래의 조건을 따르는 경우에 한하여 자유롭게

- 이 저작물을 복제, 배포, 전송, 전시, 공연 및 방송할 수 있습니다.

다음과 같은 조건을 따라야 합니다:



저작자표시. 귀하는 원저작자를 표시하여야 합니다.



비영리. 귀하는 이 저작물을 영리 목적으로 이용할 수 없습니다.



변경금지. 귀하는 이 저작물을 개작, 변형 또는 가공할 수 없습니다.

- 귀하는, 이 저작물의 재이용이나 배포의 경우, 이 저작물에 적용된 이용허락조건을 명확하게 나타내어야 합니다.
- 저작권자로부터 별도의 허가를 받으면 이러한 조건들은 적용되지 않습니다.

저작권법에 따른 이용자의 권리는 위의 내용에 의하여 영향을 받지 않습니다.

이것은 [이용허락규약\(Legal Code\)](#)을 이해하기 쉽게 요약한 것입니다.

[Disclaimer](#)

공학석사 학위논문

Fatigue Life Prediction of Thermal Barrier Coating Considering Strain–Life Relation and Crack Growth Model

변형률-수명 관계와 균열 성장 모델을 고려한 열
차폐 코팅의 피로수명 예측

2020 년 2 월

서울대학교 대학원

기계항공공학부

김연준

Fatigue Life Prediction of Thermal Barrier Coating Considering Strain--Life Relation and Crack Growth Model


변형률-수명 관계와 균열 성장 모델을 고려한 열
차폐 코팅의 피로수명 예측

지도 교수 윤 군 진


이 논문을 공학석사 학위논문으로 제출함
2019 년 12 월

서울대학교 대학원
기계항공공학부
김 연 준

김연준의 공학석사 학위논문을 인준함
2019 년 12 월

위 원 장 _____ 김 지 환 

부위원장 _____ 윤 군 진 

위 원 _____ 신 상 준 

Abstract

Fatigue Life Prediction of Thermal Barrier Coating Considering Strain–Life Relation and Crack Growth Model

Younjun Kim

Department of Mechanical and Aerospace Engineering

The Graduate School

Seoul National University

The role of the thermal barrier coating (TBC) in high temperature structures such as turbine blades is very important. Since TBCs play a role in protecting materials from extreme gas temperatures, fatigue failure of TBCs directly affects the structure's function and life. Therefore, studies on the fatigue life prediction of TBC under cyclic thermal loadings is under pressing needs. In this thesis, we investigated a methodology for the fatigue life prediction of TBC under repeated thermal loadings considering fracture mechanics. The objective of this thesis is to establish a computational

framework for the fracture mechanics–based fatigue life prediction and investigate the fatigue life under various temperature ranges.

General mechanism for materials' fatigue failure follows the initiation of the crack, propagation, and ultimately failure. Therefore, the fatigue life of TBC is predicted by sum of the number of cycles until crack initiation and the number of cycles until full separation through crack propagation. For the prediction, Morrow strain–life relation and the crack growth model proposed by Paris was adopted. In ABAQUS, J–integral values were obtained using the contour integral method to increase the accuracy of the calculations. The fatigue life cycle was calculated by post–processing and numerical integration with ABAQUS–Python script and MATLAB. In order to verify the simulation results, the results were compared with the experimental results obtained from the reference, and agreements with experimental data were confirmed within the acceptable error range. Further analysis also showed trends in fatigue life for various thermal loadings. As the temperature increases, the fatigue life decreases and the reduction gap also decreases.

Keywords : thermal barrier coating, fatigue life prediction, crack initiation, crack propagation, fracture mechanics, thermal cyclic loading fatigue

Student Number : 2018-27842

Table of contents

Abstract	i
Table of contents.....	iv
List of figures	vi
List of tables.....	vii
1. Introduction	1
1.1. Background and Motivation.....	1
1.2. Objectives and Thesis Overview.....	5
2. Life prediction method.....	7
2.1. Morrow strain–life relation (local approach)	7
2.2. Fatigue crack growth model based on fracture mechanics.....	9
3. Simulation of crack initiation and propagation.....	15
3.1. Modeling of TBC.....	15
3.2. Proposed computational procedures	18
3.3. Fatigue crack initiation.....	22
3.4. Fatigue crack propagation simulation.....	28
4. Results of simulation	33
4.1. Heat transfer and thermal loading analysis	33
4.2. Crack initiation(<i>N_i</i>) and propagation(<i>N_p</i>)	36

4.3.	Final fracture cycles(N_f).....	38
4.4.	Comparison between experiment and simulation	39
4.5.	Fatigue life under various temperature loading.....	41
5.	Conclusion and future works	48
5.1.	Conclusion.....	48
5.2.	Future works	49
6.	Reference	51
	국문초록.....	58

List of figures

FIGURE 1. MORROW STRAIN-LIFE RELATION	8
FIGURE 2. CRACK GROWTH RATE CURVE.....	12
FIGURE 3. MECHANISM OF SPALLATION	16
FIGURE 4. 3D MODEL OF TBC.....	17
FIGURE 5. GENERATED MESH OF TBC.....	18
FIGURE 6. OVERALL FLOW CHART OF SIMULATION	21
FIGURE 7. EXAMPLE OF LOG SCALE LIFE CONTOUR.....	27
FIGURE 8. PARIS' LAW GRAPH BETWEEN da/dN AND ΔK	29
FIGURE 9. PREDICTED CRACK PATH USING XFEM.....	30
FIGURE 10. RESULTS OF J-INTEGRAL ; A) CONTOUR INTEGRAL ; B)XFEM	32
FIGURE 11. RESULT OF HEAT TRANSFER ANALYSIS (TEMPERATURE CONTOUR).....	34
FIGURE 12. RESULT OF THERMAL LOADING ANALYSIS (STRESS CONTOUR)	35
FIGURE 13. RESULT OF FE-SAFE SIMULATION (LOG LIFE CONTOUR).....	36
FIGURE 14. COMPARISON EXPERIMENT DATA VS SIMULATION DATA.....	40
FIGURE 15. HEAT TRANSFER ANALYSIS AT (A) 900°C; (B) 1000°C; (C) 1200°C.....	42
FIGURE 16. THERMAL LOADING ANALYSIS AT (A) 900°C; (B) 1000°C; (C) 1200°C.....	43
FIGURE 17. CRACK INITIATION CYCLE ANALYSIS AT (A) 900°C; (B) 1000°C; (C) 1200°C	44
FIGURE 18. FATIGUE LIFE FOR VARIOUS THERMAL LOADING.....	47

List of tables

TABLE 1. HEAT TRANSFER PROPERTIES OF TBC	22
TABLE 2. THERMAL LOADING ANALYSIS PROPERTIES OF TOP COAT.....	23
TABLE 3. THERMAL LOADING ANALYSIS PROPERTIES OF TGO.....	24
TABLE 4. THERMAL LOADING ANALYSIS PROPERTIES OF BOND COAT.....	25
TABLE 5. CONSTANTS OF MORROW EQUATION	26
TABLE 6. RESULT OF FE-SAFE SIMULATION	37
TABLE 7. RESULT OF NUMERICAL INTEGRATION FOR CRACK PROPAGATION LIFE.....	37
TABLE 8. FINAL FRACTURE CYCLES.....	38
TABLE 9. EXPERIMENTAL RESULTS	40
TABLE 10. CRACK INITIATION CYCLE FOR VARIOUS THERMAL LOADING	45
TABLE 11. CRACK PROPAGATION CYCLE FOR VARIOUS THERMAL LOADING	45
TABLE 12. FINAL FRACTURE CYCLE FOR VARIOUS THERMAL LOADING	46

1. Introduction

1.1. Background and Motivation

The thermal barrier coating (TBC) used for turbine blades protects the gas turbine from high-temperature gases. However, TBC is exposed to cyclic thermal loading conditions where high and low temperatures are repeated, causing repeated thermal deformation to reach failures over times. The failure of TBC can be regarded as a failure of the turbine blades because the failure of TBC is very fatal to turbine blades [1, 2]. Therefore, the fatigue life prediction of TBC is one of the most critical factors in the design of turbine blades. Life expectancy of materials has been steadily studied in various approaches [1, 3–6]. As the most common method, various methods are proposed, ranging from life prediction using the SN curve to fracture mechanics-based life prediction considering the crack growth.

The general fatigue life prediction method is divided into 1) Global S–N approach, 2) Local approach through strain–life and

stress–life models or 3) fracture mechanics–based fatigue life prediction as mentioned above [7]. The first, global S–N approach derives the relationship between stress range ($\Delta\sigma$) and the total number of cycles to failure (N_f) through the most common fatigue tests using specimens [8–11]. The S–N data is applied to the result of stress analysis of the whole structure to predict the life of the whole structure. However, the global S–N approach is conservative and limited because it does not reflect structural geometry and material specifications. Local approach is associated with local failures such as crack initiation. The number of crack initiation cycles at the hot spot is predicted by the strain–life or stress–life relationship [12]. Morrow’s equation is one that represents the local strain–life models [13]. Material parameters required for Morrow’s model can be obtained by curve fitting of the elastoplastic stress–strain curve using simplified constitutive model such as Ramberg–Osgood model [14]. Because global and local approach models perform conservative prediction, alternative methods such as fracture mechanics based models have also been proposed [11, 15–18]. The fracture mechanics–based models need simplified formulae

of the stress intensity factor, which are often provided in standard handbooks [19]. Paris law correlating da/dN with ΔK has been applied to a number of studies [20–23] as a reliable lifetime prediction model ever since it was proposed [24]. But it has limitations in explaining unstable crack propagation regime, crack closure [23], and the effect of stress ratio. Several modified models have been suggested, by Forman et al. [25], Erdogan and Ratwani [26], Forman and Mettu [27], NASGRO [28], Agha et al. [29], Chantier et al. [30], etc. The models suggested by Forman and Mettu [27] and NASGRO [28] provided the crack growth rate over the full range of the stress intensity factor from the threshold to the critical value at instability. In addition, they can take into account effects of the stress ratio, the ratio of applied stress to the yield strength and the plasticity induced crack closure [31].

Typical TBC consists of ceramic top coat (TC), metallic bond coat (BC), substrate and thermally grown oxide (TGO). TGO is a layer formed between TC and BC by being oxidized under thermal loading. [32] This TGO causes stress between TC and TGO or between TGO and BC due to expansion difference, which leads to

crack initiation.[1, 33] Therefore, the TGO growth rate must be considered to predict the failure of the entire TBC.[34] TBC is classified into physical vapor deposition (EB-PVD) or atmospheric plasma-spraying (APS). EB-PVD coatings have long life due to excellent strain tolerance but are expensive.

de Jesus, et al. combined the local fatigue life prediction approach with the fracture mechanics-based method to predict the total fatigue life of riveted and bolted joints by $N_f = N_i + N_p$ [7]. N_i is the number of cycles until macroscopic fatigue crack initiation and N_p is the number of cycles until complete separation of structural members through fatigue crack propagation.[35] They determined the stress intensity factor by means of the Virtual Crack Closure Technique (VCCT) [36] considering clamping stress and frictions between plate members. Similar approach was attempted in literatures with emphasis on uncertainties associated with clamping and friction actions [37].

1.2. Objectives and Thesis Overview

In this thesis, we attempt to predict fatigue life of TBC subjected to cyclic thermal load through fracture mechanics-based simulation. The local approach predicted the crack initiation cycle and predicted the crack propagation cycle through crack growth model based on fracture mechanics to predict the number of life cycles until the final failure occurred. And the validity was verified by comparing the fatigue life cycle number through simulation with the experimental results obtained from the reference.

Modeling of TBC and heat transfer & thermal loading analysis was performed by ABAQUS. Thermal loading analysis was performed by applying the thermal gradient data from the heat transfer analysis. The stress-strain data resulting from thermal loading analysis was imported to FE-safe in the form of *.odb file and the prediction of crack initiation cycle was performed through the strain-life relation. Morrow strain-life relation was adopted as strain-life model. Also ABAQUS was used to define cracks in the same TBC geometry to obtain J-integral values for each crack stage. This J-integral value is post-processed and subjected to numerical

integration based on crack growth model to perform prediction of crack propagation cycle. ABAQUS–Python script was used for J–integral post–processing, and all processes including numerical integration and submitting ABAQUS input files were done in script form in MATLAB. The number of final failure cycle, obtained by summing the crack initiation cycle and the propagation cycle, was validated against the experimental data of the reference.

2. Life prediction method

2.1. Morrow strain-life relation (local approach)

Crack initiation to predict the fatigue life, a proper local approach model is required, and corresponding physical property values are required. The local approach is to find out the fatigue life at each spot using the S–N curve. Fatigue life at each spot is obtained through matching stress (or strain) data to the S–N curve. Depending on the model, a stress–life relation or strain–life relation is used. In this thesis, Morrow strain–life relation was used as the local approach. The Morrow strain–life model is a model in which the mean stress effect correction is applied to the Manson–Coffin equation [20]. Manson–Coffin equation is as followed.

$$\frac{\Delta\varepsilon}{2} = \frac{\sigma'_f}{E} (2N_f)^b + \varepsilon'_f (2N_f)^c \quad (1)$$

where, σ'_f is fatigue strength coefficient, b is fatigue strength exponent, ε'_f is fatigue ductility coefficient, c is fatigue ductility exponent, and N_f is the number of failure cycle. A graph of the Morrow equation is shown in Figure 1.

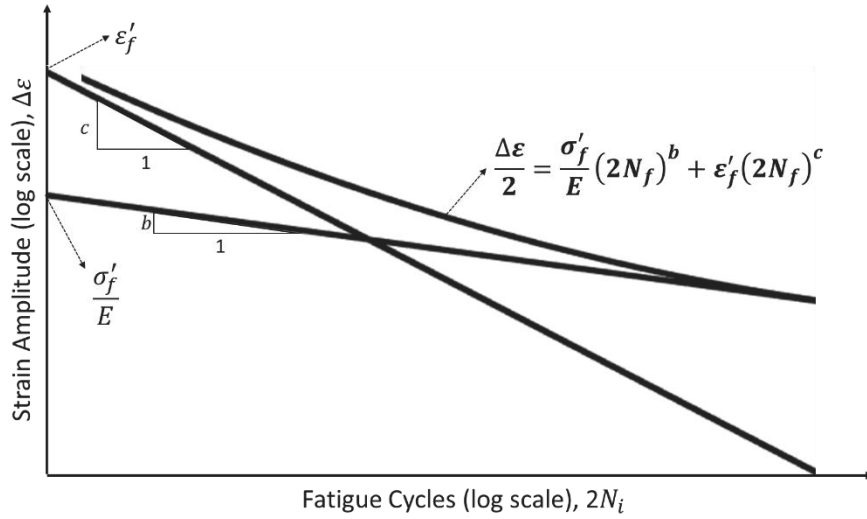


Figure 1. Morrow strain-life relation

Most materials or structures under cyclic loading are generally affected by mean stress values [38]. Mean stress (σ_m) means the average value of maximum stress (σ_{max}) and minimum stress (σ_{min}) in cyclic loading. σ_m may be expressed as follows.

$$\sigma_m = \frac{\sigma_{max} + \sigma_{min}}{2} \quad (2)$$

However, the conventional Morrow equation does not consider the mean stress effect. Without considering the mean stress effect, fatigue life can be assessed conservatively or non-conservatively. For example, when the mean stress is a tensile stress (greater than 0 value), the fatigue life is smaller than value estimated by the

conventional model. Mean stress effects in strain–life relation have been steadily studied [39]. Mean stress effect correction methods vary [23], in case of Morrow strain–life relation [40] the elastic term was modified by subtracting the mean stress (σ_m). Morrow strain–life is as followed.

$$\frac{\Delta\varepsilon}{2} = \frac{(\sigma_f' - \sigma_m)}{E} (2N_f)^b + \varepsilon_f' (2N_f)^c \quad (3)$$

2.2. Fatigue crack growth model based on fracture mechanics

Fatigue life predictions based on LEFM are usually predicted through fracture parameters such as the stress intensity factor range ΔK . In Paris law, the relationship between ΔK and fatigue crack growth rate, da/dN , is presented first in the literature [37]. The equation is expressed as follows.

$$\frac{da}{dN} = C_p \Delta K^{m_p} \quad (4)$$

where C_p and m_p are material constants from fatigue crack

propagation tests of the base material; ΔK is the stress intensity factor range. There is a threshold value of the stress intensity factor range (ΔK_{th}), below which no fatigue crack propagation occurs. The stress intensity factor is a basic physical quantity in LEFM, which is related to applied load, crack geometry and crack size as

$$\Delta K = \Delta\sigma Y\sqrt{\pi a} \quad (5)$$

Where $\Delta\sigma$ is the stress range, Y is the geometry function, and a is the fatigue crack size. There is a threshold value (ΔK_{th}) for the stress intensity factor in the long crack regime, which is a border between propagating and non-propagating crack size. If the applied stress intensity factor is greater than ΔK_{th} , then the crack can grow by fatigue. Then the number of cycles from the initial crack size (a_i) to the final crack size (a_f) is computed by integrating Eq. (4) as follows

$$\begin{aligned}
N_p &= \frac{1}{C_p} \int_{a_i}^{a_f} \frac{1}{\Delta K^{m_p}} da = \frac{1}{C_p (\Delta \sigma)^{m_p} Y^{m_p} \pi^{m_p/2}} \int_{a_i}^{a_f} a^{-m_p/2} da. \\
&= \frac{1}{C_p (\Delta \sigma)^{m_p} Y^{m_p} \pi^{m_p/2}} \frac{a_i^{1-m_p/2} - a_f^{1-m_p/2}}{\frac{m_p}{2} - 1}
\end{aligned} \tag{6}$$

The final crack size (a_f) depends on either geometrical thickness giving the net section or material toughness that determines the maximum stress intensity factor. Actual computation of the integration Eq. (6) is approximately performed assuming a constant stress intensity factor at the beginning of the crack increment as follows

$$\Delta N_p = \frac{1}{C_p} \frac{1}{\Delta K^{m_p}} \Delta a. \tag{7}$$

However, the stress intensity factor is a function of the crack size, which is computed by VCCT in the finite element model.

The crack growth rate for typical materials is divided into three regimes as shown in Figure 2. When the stress intensity factor is below the threshold stress intensity factor range ΔK_{th} , no crack growth is observed. However, in Regime III, when ΔK approaches to

the asymptote (K_c), the crack growth is accelerated. In Eq. (4), C is the intercept constant having a unit $(\text{mm/cycle})(\text{MPa}\sqrt{\text{m}})^{-n}$ and m_p is the slope of $\log(da/dN) - \log(\Delta K)$ curve.

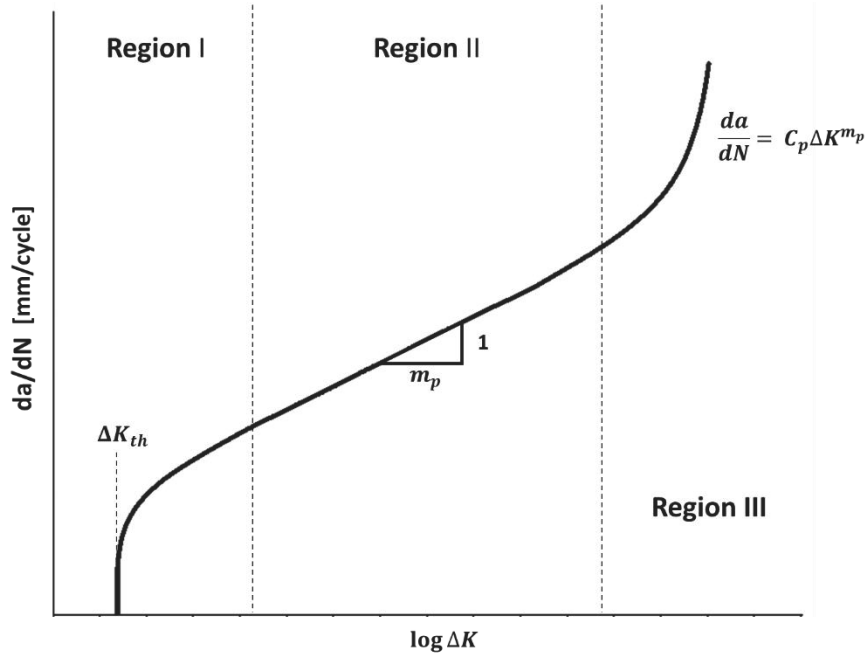


Figure 2. Crack growth rate curve

As the stress ratio ($R = \frac{\sigma_{\min}}{\sigma_{\max}}$ or $\frac{K_{\min}}{K_{\max}}$) increases, the $\log(da/dN) - \log(\Delta K)$ curve becomes shifted to upper region, which means that fatigue crack growth rate increases. Especially, when $R=0$ corresponding to zero-to-tension loading, the vertical asymptote becomes the critical stress intensity (K_c same as the

fracture toughness) for the material with a relationship of $\Delta K = K_{\max}(1 - R) = K_c(1 - R)$. Because the original Paris law model in Eq. (5) is incapable of reflecting the stress ratio effect, Walker proposed a modified linear model as follows [41].

$$\frac{da}{dN} = C_0 \left(\frac{\Delta K}{(1 - R)^{1-\gamma}} \right)^n \quad (8)$$

Where R is the stress ratio and C_0 is the intercept constant corresponding to the stress ratio $R=0$. The value γ is a constant that determines how strongly the stress ratio R influences the fatigue crack growth rate. The original Paris law and Walker's model can describe Regime II well, but they cannot fully implement the other two regimes. NASGRO model equation is one of the full-range models that cover Regimes I, II and III [42–44]. It is expressed as follows

$$\frac{da}{dN} = C_0 \left[\left(\frac{1-f}{1-R} \right) \Delta K \right]^n \frac{\left(1 - \frac{\Delta K_{th}}{\Delta K} \right)^p}{\left(1 - \frac{K_{max}}{K_c} \right)^q} \quad (9)$$

Where p and q are constants describing the curvature near the threshold Regime I and near instability Regime III, respectively. f is

the crack opening function, which is used to model the influence of various crack closure mechanism [45]. NASGRO model was modified by Maierhofer et al. [42] for describing crack growths of arbitrary length and accounting for short crack effects through a new crack opening function. On the other hand, Forman proposed an extension of the Walker model reflecting Regime III [46], and Hartman and Schijve extended the Forman equation to consider all three crack propagation regimes [47]. The equation is as follows.

$$\frac{da}{dN} = \frac{C \cdot (\Delta K - \Delta K_{th})^m}{(1 - R)K_{max} - \Delta K} \quad (10)$$

However, this early version of fatigue crack propagation model does not include the stress ratio dependency of ΔK_{th} . Integration of the fatigue crack growth model is common to all of existing models from the initial crack size (a_i) to estimate the fatigue life. The initial crack length is assumed equal to EIFS that is challenging to define. It is often estimated by Kitagawa–Takahashi diagram inflection points [48].

3. Simulation of crack initiation and propagation

3.1. Modeling of TBC

Many methods of 3d modeling thermal barrier coating have already been studied.[4, 34, 49] In general, the substrate is not considered because stresses in the coating are governing the lifetime and mainly cracks are formed between top coat and TGO. Therefore, only top coat, TGO, and bond coat were considered in 3d modeling. Most cycles of TBC failure regarded as cycle when spallation occurs.[50] The mechanism of spallation is briefly described in the Figure 3. In general, when TGO is formed, it is formed as a very non-uniform surface rather than a flat surface. Therefore, many studies have conducted modeling by forming uniform bends. And as mentioned above, the thickness of TGO has a very important effect, which is modeled between the top coat and the bond coat by offsetting the constant curve by the thickness of TGO. The thickness of TGO is defined by experimental results from reference.[32] As will be mentioned later, the thickness of TGO will grow with increasing crack stages. The structure of the modeled TBC is shown in Figure 4.

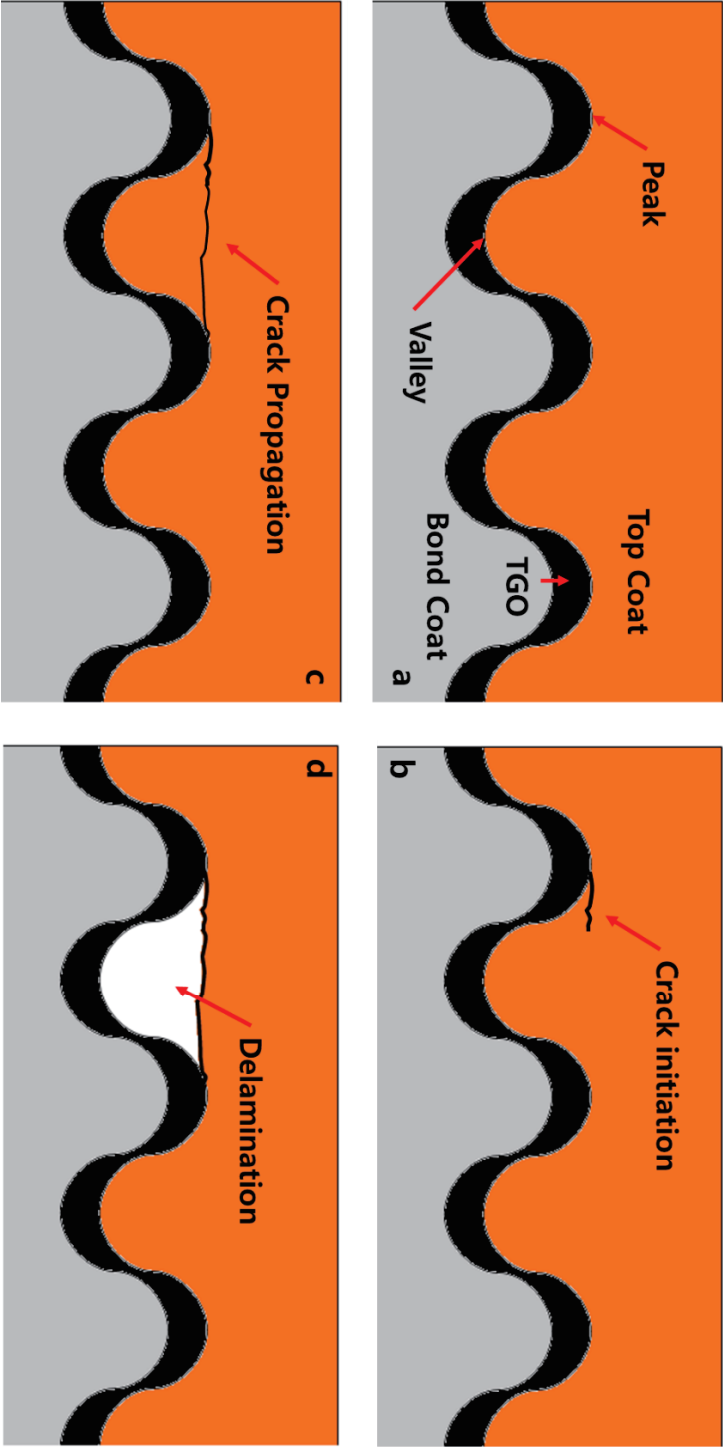


Figure 3. Mechanism of spallation

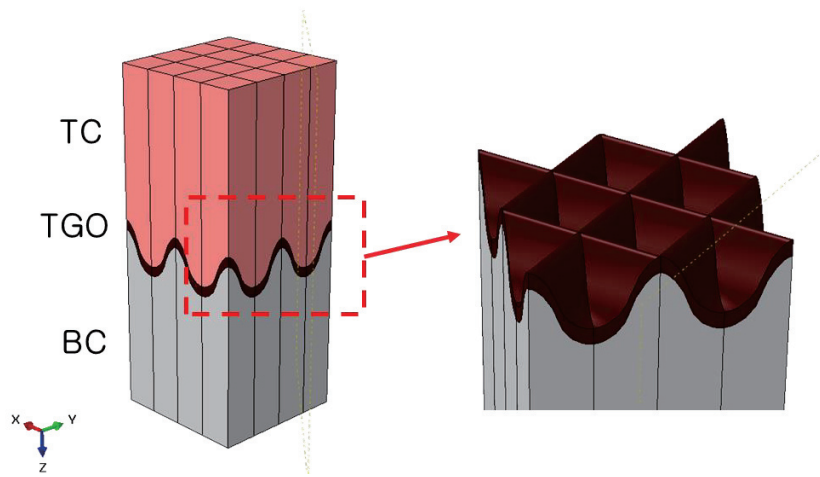


Figure 4. 3d model of TBC

The mesh was formed by dividing the repeated pattern into 16 cells to produce a uniform hexahedral mesh. In addition, the refinement was performed around the TGO layer where cracks are generated. The ideal mesh configuration for mapping thermal gradients from heat transfer analysis to thermal loading analysis is to generate same mesh for each analysis. Therefore, the mesh configuration of the heat transfer analysis and the thermal loading analysis were generated identically. The number of elements is 138720. The generated mesh is shown in Figure 5.

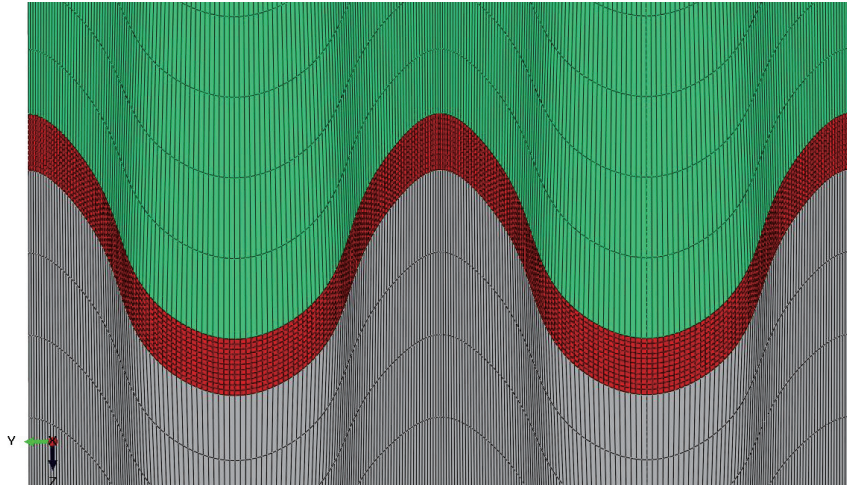


Figure 5. Generated mesh of TBC

3.2. Proposed computational procedures

There are two major steps taken in this thesis, which are corresponding to crack initiation and fatigue crack propagation simulations. From these two steps, we finally get the number of cycles N_i and N_p and sum them up to obtain the final fatigue life cycle. Detailed procedures are illustrated in Figure 6.

- Detailed computational procedures
 - i) Finite element models for actual specimens with voids were developed by using ABAQUS CAE
 - ii) Crack initiation
 - (1) We subject the FE model to cyclic loading in order to obtain the stress contour.
 - (2) Stress contour information in *.odb file is imported to the FE-safe to obtain the contour of the fatigue life. From the fatigue life contour, we locate the hot spot and the worst life cycle is obtained.
 - iii) Crack propagation
 - (1) We identify the worst life spot and define the crack.
 - (2) Apply heat to the top coat surface to conduct heat transfer analysis to obtain thermal gradient of the entire structure.
 - (3) Apply the obtained thermal gradient to the structure and conduct thermal loading analysis.

- (4) We obtain J-integral values at the location of cracks
 - (5) Importing J-integral values to MATLAB, numerical integration is performed in the fatigue crack growth model. ABAQUS python script was used to import J-integral value to MATLAB environment.
 - (6) While increasing the crack size and thickness of TGO, “iii-1” to “iii-3” steps are repeated until the final separation.
 - (7) N_p is obtained from the numerical integration if the crack reaches final separation.
- iv) Finally, the fatigue life (N_f) from the beginning to the final separation is obtained by summing up N_i and N_p .

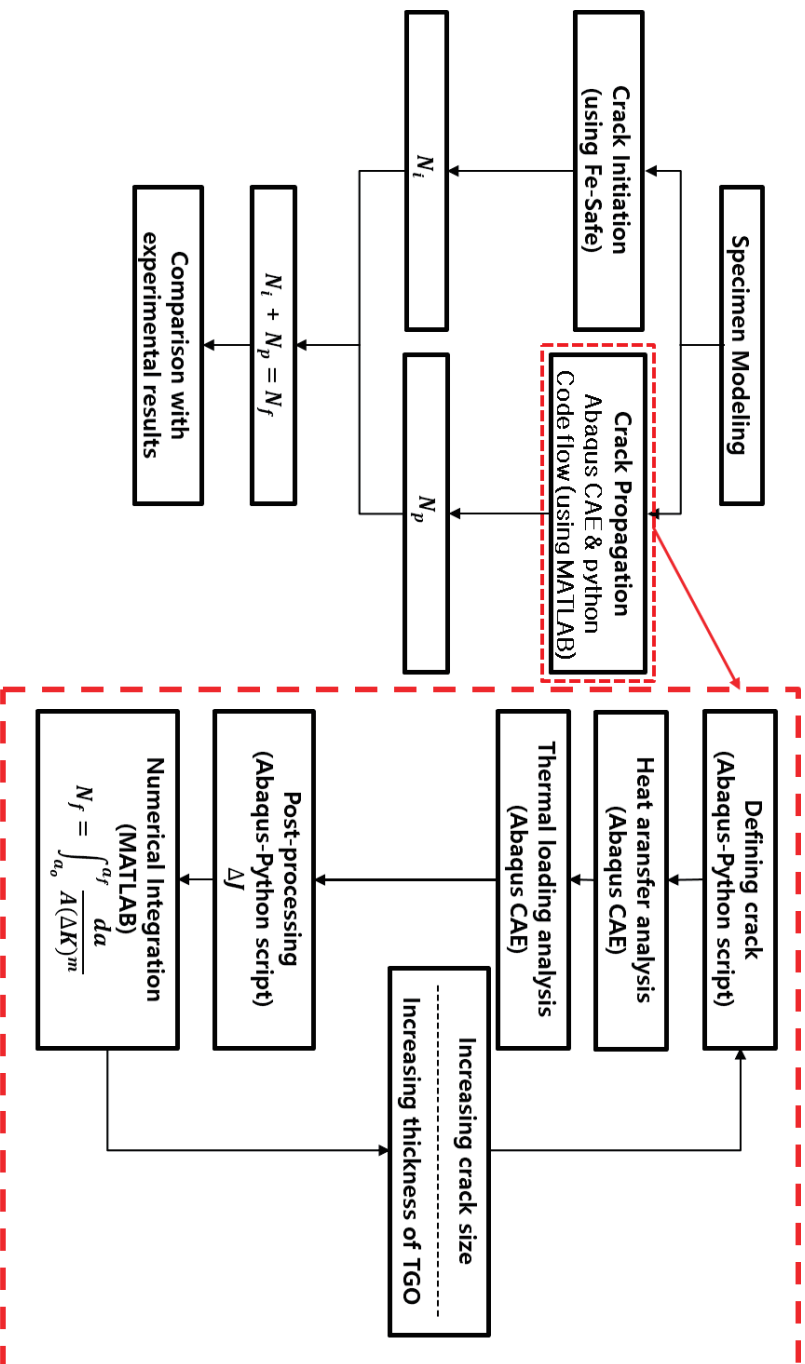


Figure 6. Overall flow chart of simulation

3.3. Fatigue crack initiation

As mentioned above, FEM analysis should be the first to predict crack initiation and crack propagation life. First, heat transfer analysis to obtain the thermal gradient of the entire structure requires thermal conductivity, specific heat, and density. And the thermal loading analysis by applying the obtained thermal gradient requires elastic properties (Young's Modulus, Poisson's ratio) and thermal expansion coefficient.[51] In particular, because of thermal loading rather than general mechanical loading, temperature dependent properties are required for more accurate thermal loading analysis. [51]

Table 1. Heat transfer properties of TBC

Layers	Thermal conductivity ($W m^{-1} K^{-1}$)	Specific heat ($J K^{-1}kg^{-1}$)	Density (kg/m^3)
TC	2.5	400	5.85e3
TGO	1.3	680	2.65e3
BC	30	900	2.70e3

Table 2. Thermal loading analysis properties of top coat

Temperature (°C)	$\alpha (\times 10^{-6}\text{°C}^{-1})$	$E(\text{GPa})$	ν
28		65	0.1
200	10.2	56	0.1
300		58	0.1
400		54	0.1
500		53	0.1
650	9.78	44	0.11
760		40	0.11
850	10.02	31	0.11
980	10.34	29	0.12
1050		23	0.12
1100	10.29	18	0.12

Table 3. Thermal loading analysis properties of TGO

Temperature (°C)	$\alpha (\times 10^{-6}\text{°C}^{-1})$	$E(\text{GPa})$	ν
28	8.2	400	0.23
200			
300			
400	8.4	390	0.23
500			
650	8.7	380	0.24
760			
850	9	355	0.25
980	9.3	325	0.25
1050			
1100	9.6	320	0.25

Table 4. Thermal loading analysis properties of bond coat

Temperature (°C)	$\alpha (\times 10^{-6}\text{°C}^{-1})$	$E(\text{GPa})$	ν
28		198	0.31
200			
300			
400		189	0.32
500	20.5	162	0.32
650		151	0.33
760		143	0.33
850		134	0.34
980	24.3	129	0.34
1050		124	0.35
1100	34.2	119	0.37

In this thesis, the number of cycles until the crack initiation was predicted using the strain–life relation. In order to predict the crack initiation, the material constants of the Morrow equation σ'_f , b , ϵ'_f , and c should be determined. The Morrow equation constants of are summarized in Table 5.[2]

Table 5. Constants of Morrow equation

σ'_f (MPa)	b	ϵ'_f	c
1430	-0.182	0.63	-0.88

The number of cycles until the crack initiation was predicted using Fe–Safe ABAQUS suite software. At first, FE analysis was performed by Abaqus CAE using the properties given in As mentioned earlier, FE analysis is divided into heat transfer analysis and cyclic thermal loading. Apply a 1373K (1100 °C) condition such as hot gas temperature to the surface of the top coat, and conduct a heat transfer analysis to obtain a thermal gradient throughout the structure. The results of heat transfer analysis are used as input for thermal loading analysis in the form of .odb files. When the analysis

is performed under the obtained thermal gradient condition, the stress and strain data for the corresponding thermal loading are also obtained in the form of .odb file. Importing the odb file into Fe-safe, a fatigue life contour based on the stress (or strain) data is obtained. Various fatigue life models can be selected within Fe-safe. In this thesis, Morrow strain-life equation was adopted and the properties shown in Table 5 were used. The Fe-safe provides the fatigue life contour (log scale) based on the odb file data obtained from FE simulations under a cyclic loading. The example of fatigue life contour is shown in Figure 7. The loads were repeatedly applied in the form of sinusoidal function. The number of loading cycles was 10^8 . As can be seen in Figure 7, the areas with zero value of stress (or strain) show a life of 8 on a log scale. Crack initiation occurred at the position having the worst life and that life was adopted as a life until crack initiation.

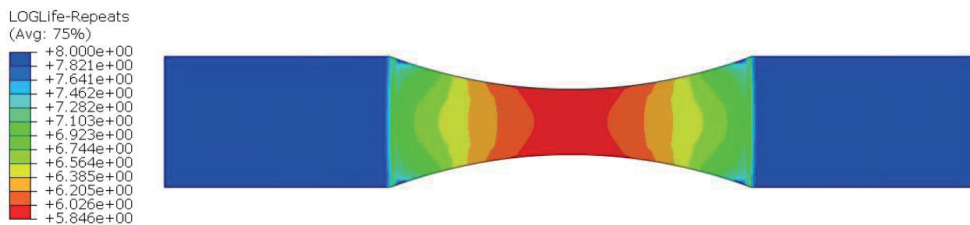


Figure 7. Example of log scale life contour

3.4. Fatigue crack propagation simulation

In this thesis, Paris' law using most commonly as crack growth model is adopted. Although this model has a limit that does not reflect the specific threshold value of ΔK , it is sufficient to consider only region II in Figure 2 because the initiation cycle and spot have already been predicted. This process requires crack growth experiment data. In this thesis, we found the relation $da/dN = 10^{-18.09} \cdot \Delta K^{22.24}$, which is a relation between da/dN and ΔK of top coat (YSZ). Based on the graph image presented in the reference, the coefficient of Paris' law was obtained. [3] The graph between da / dN and ΔK relation is shown as Figure 8.

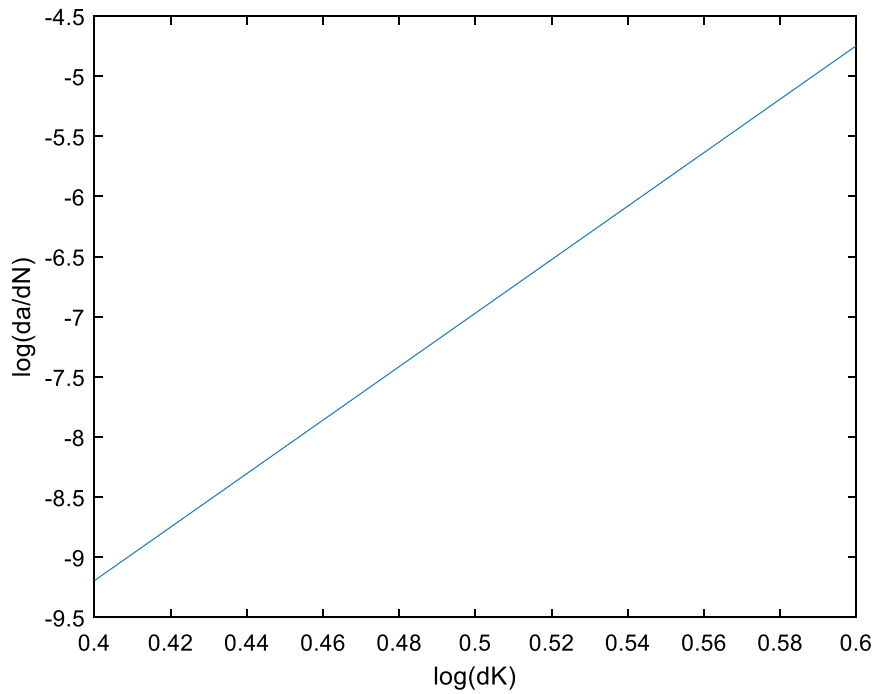


Figure 8. Paris' law graph between da/dN and ΔK

The crack propagation process was performed by applying Abaqus CAE and Abaqus–python to MATLAB based on the crack growth model. The modeling process was done, using ABAQUS CAE. Mesh refinement was performed around the crack tip area to obtain accurate results.

As crack is propagated, the J–integral value at the corresponding crack stage is extracted through contour integral. To obtain the J–

integral value in the crack tip, we used the shell element along the crack path from the crack initiation point. The crack path was found in advance by crack growth using XFEM in ABAQUS from the initiation point. As shown in the Figure 3, the crack propagates along direction from peak of initiation spot to other peak. The predicted crack path using XFEM is shown in the Figure 9.

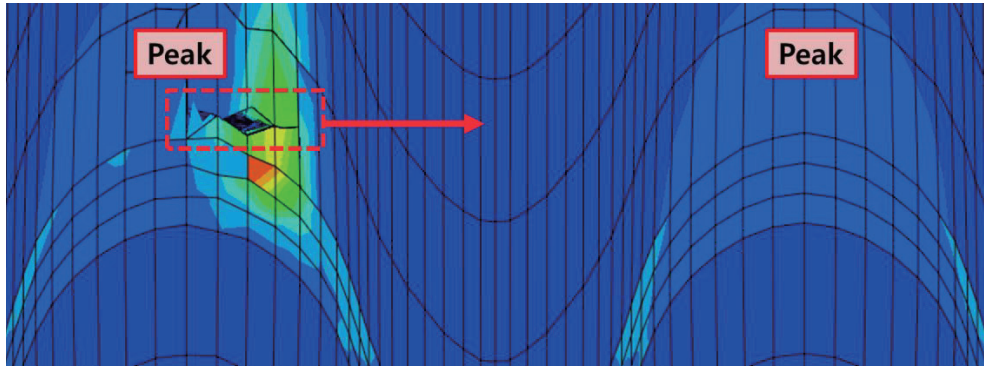


Figure 9. Predicted crack path using XFEM

The modeling process applying developing crack to the structure was carried out using the ABAQUS–Python script. The J–integral values from the corresponding crack stages were calculated by post processing, and numerical integration was performed by substituting these values into the Paris' law.

The J–integral extraction method is largely divided into contour integral and XFEM method in ABAQUS. In the case of the contour integral method, when the crack position is known in advance, a circular mesh is formed around the crack tip to obtain fracture mechanics parameters such as stress intensity factor and J–integral. On the other hand, XFEM method obtains fracture mechanics parameter by creating new element suitable for crack even if crack tip part is formed regardless of mesh shape. Therefore, the XFEM method, which requires the creation of a new element centered on cracks, takes a relatively long computation time. However, in this thesis method, since the location of the crack is known in advance, contour integral method has the advantage of reducing computation time. Therefore, J–integral values were obtained using the contour integral method. The results of J–integral obtained by contour integral and XFEM method for the same crack are compared and shown in the Figure 10. If the location of the crack is correct, the contour integral method generally converges better and is accurate.

J - INTEGRAL ESTIMATES (a)						
CRACK NAME	CRACKFRONT NODE SET	CONTOURS				
		1	2	3	4	5
CRACK-1	XFEM_1	5738.	3651.	4656.	4493.	4439.
	XFEM_2	6068.	4294.	3918.	3866.	3888.

J - INTEGRAL ESTIMATES (b)						
CRACK NAME	CRACKFRONT NODE SET	CONTOURS				
		1	2	3	4	5
H-OUTPUT-1_CRACK-1	-4-	3002.	3485.	3484.	3484.	3484.
	-5-	3002.	3485.	3484.	3484.	3484.

Figure 10. Results of J-integral ; a) contour integral ; b)XFEM

All computation processes except geometry modeling were done in MATLAB script. Because of the characteristics of the ceramic, the plasticity was ignored and the analysis was conducted only in the elastic range. So the following relation holds between ΔK and ΔJ .

$$\Delta J = \frac{\Delta(K)^2}{E} \quad (11)$$

4. Results of simulation

4.1. Heat transfer and thermal loading analysis

The results of the heat transfer analysis are shown in Figure 11. As expected, the thermal gradient gradually decreases as the temperature goes down to the TGO from the top coat where the heat is applied, and the change in temperature in the bond coat is virtually not significant. In practice, the thermal gradient applied to the structure changes slightly as the crack develops, but because the cracks in ABAQUS are considered to be in contact with the surfaces, the thermal gradient at each crack stage is same.

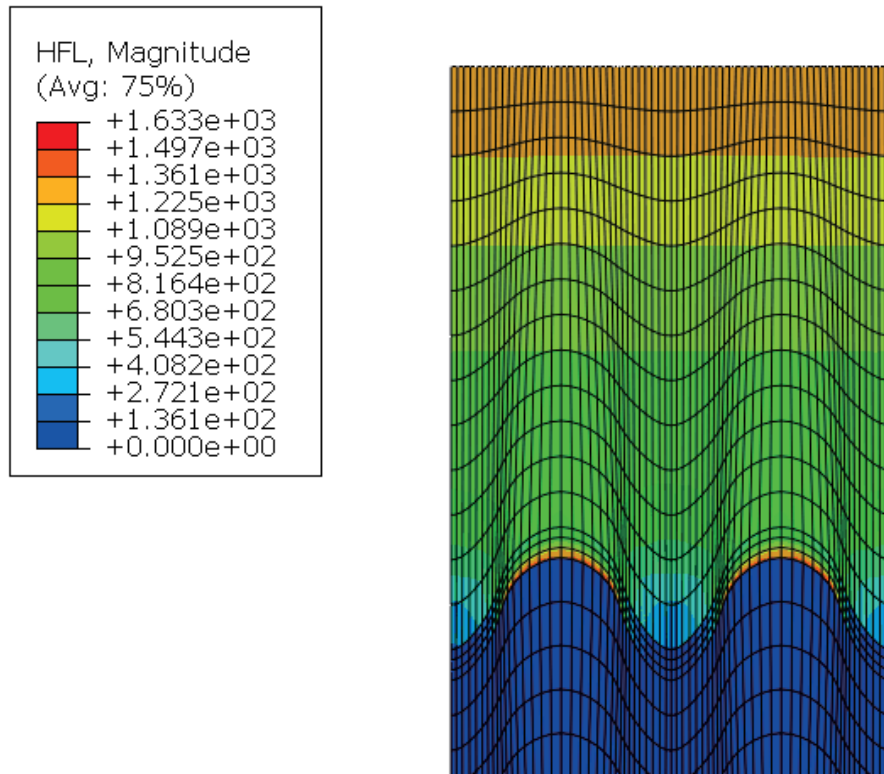


Figure 11. Result of heat transfer analysis (temperature contour)

Thermal loading analysis is performed by inputting the thermal gradient of the entire structure from the heat transfer analysis. After the thermal loading analysis is completed, the stress contour of the entire structure is shown in the Figure 12. It can be seen that the high stress is formed at the peak of TGO by thermal loading.

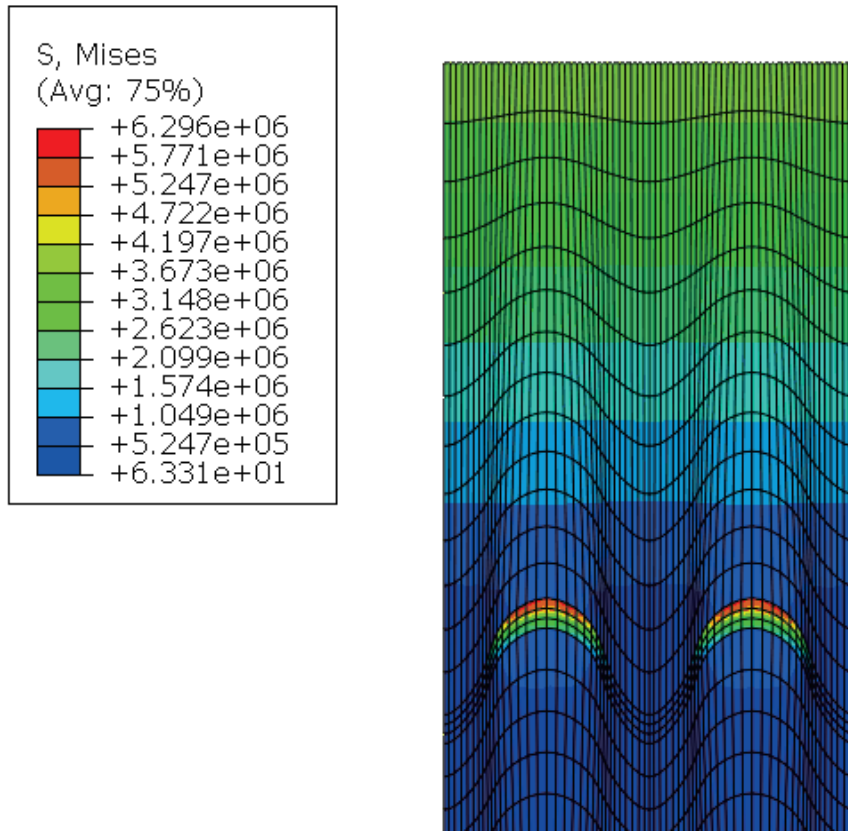


Figure 12. Result of thermal loading analysis (stress contour)

4.2. Crack initiation(N_i) and propagation(N_p)

The stress–strain data was obtained through FEM analysis. The results of fe–safe analysis using this data are shown in Figure 13 and Table 6. Fe–safe's analysis results are shown in the form of life contours (log scale) as shown in the figure, and find the worst life cycle and spot through the life contour. As shown in the figure, the worst life occurs at the peak of the TC / TGO interface.

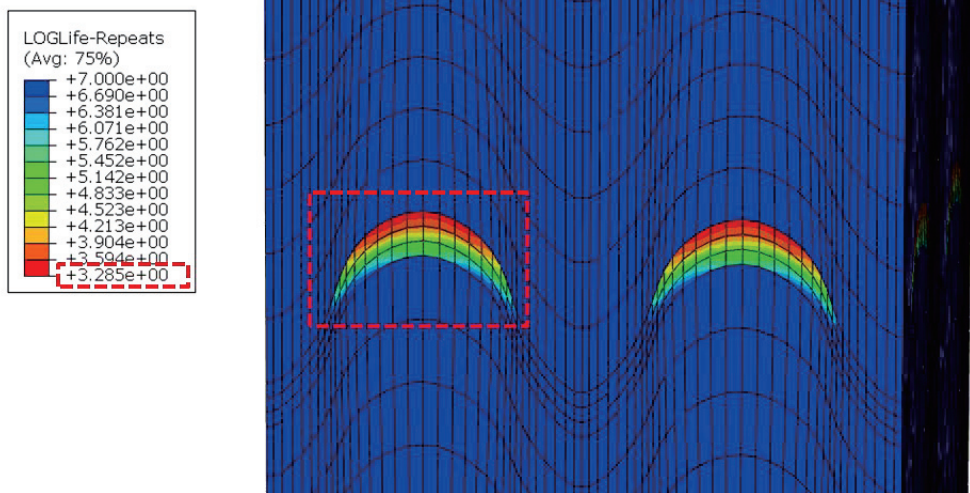


Figure 13. Result of fe-safe simulation (log life contour)

Table 6. Result of fe-safe simulation

Log life	Actual life(N_i)
3.285	1927.52 cycles

Table 7 shows the results of numerical integration using ABAQUS and MATLAB assuming cracks manually at the crack initiation spots obtained through fe-safe analysis. The number of cycles shown in the figure is the number of cycles from crack initiation to final fracture.

Table 7. Result of numerical integration for crack propagation life

Crack propagation life(N_p)
783 cycles

4.3. Final fracture cycles(N_f)

As mentioned above, the cycle in which the structure or specimen finally breaks is determined by the sum of cycles considering crack initiation cycle and crack propagation. Therefore, the final fracture cycle was predicted through the sum of the results obtained through FE-safe and crack growth models. Table 8 shows the final fracture cycles calculated through simulation and experiment data.

Table 8. Final fracture cycles

Crack initiation life (N_i)	Crack propagation life (N_p)	Total (N_f)
1581.25 cycles	783 cycles	2710.52 cycles

4.4. Comparison between experiment and simulation

Experimental results to compare with the results of simulations are studied in previous study. In general, the experiments on plasma sprayed thermal barrier coating systems were most frequently performed, and the simulation also used with mechanical properties of plasma sprayed thermal barrier coating. Although the top coat, TGO, and bond coat materials differ slightly depending on types of TBC, mechanical properties of TBC were not much different. Especially YSZ is mostly adopted as top coat material. Thermal cyclic fatigue tests were performed at the maximum temperatures of 1100 °C as in the simulation.

Since the properties and environment of simulation and experiment cannot be exactly the same, the results were compared with several experimental results. The number of failure cycles is only given in the form of a graph of log scale, so coordinate values is obtained based on the graph image. Several experimental results are shown in the Table 9.

The number of final fracture cycles obtained through the simulation is compared with the experimental data obtained from the reference. The results are shown in Figure 14. [5, 32, 52, 53]

Table 9. Experimental results

Experiment model	Log life	Actual life
Trunova et al.[52]	3.3517	2247.50
Krishna et al.[53]	3.306	2023.02
Bargraser et al. (hold 1hour) [5]	2.5884	387.61
Miller et al. (hold 1hour) [32]	2.1779	150.63

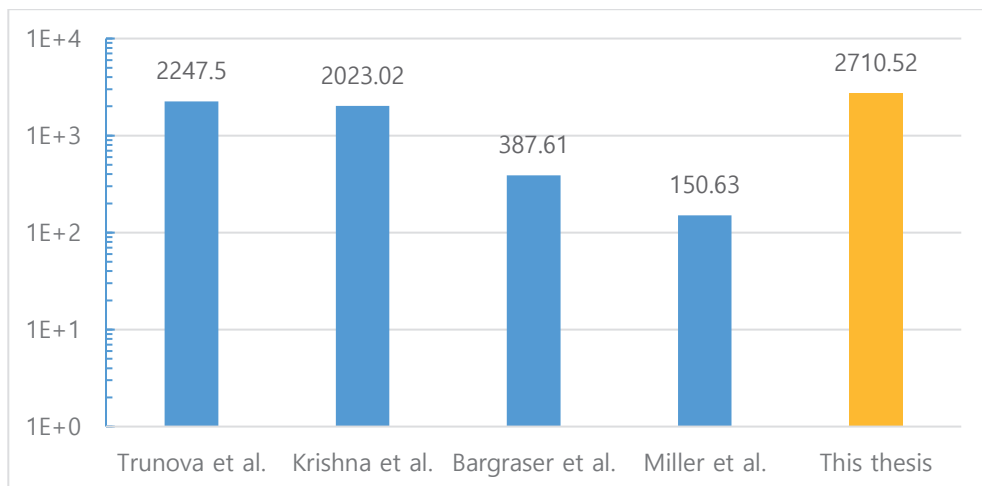


Figure 14. Comparison experiment data vs simulation data

Although it is conservative compared to other experiments, it can be seen that similar values are generally obtained. In particular, Baargraser et al. and Miller et al. In this case, the experiment was conducted after exposing it to heat for a certain time, and it can be seen that the life was shorter than other cases.

4.5. Fatigue life under various temperature loading

In order to examine the shape of the S–N curve, additional simulations were performed for various thermal loading. All models were analyzed for crack initiation cycle and crack propagation cycle. Finally, final fracture cycle was obtained. In order to reduce the computation time, all models reduced the number of crack stages. In addition to the 1100 °C previously analyzed, the analysis was further performed at 900 °C, 1000 °C, 1200 °C. The results of FEM analysis and fe-safe analysis for each temperature are shown in Figure 15 and Table 10~12. As the thermal loading increased, the number of fatigue life cycles decreased. In particular, the smaller thermal loading, the greater the amount of reduction in fatigue life cycle. The results for various thermal loading are shown in the Figure 18 .

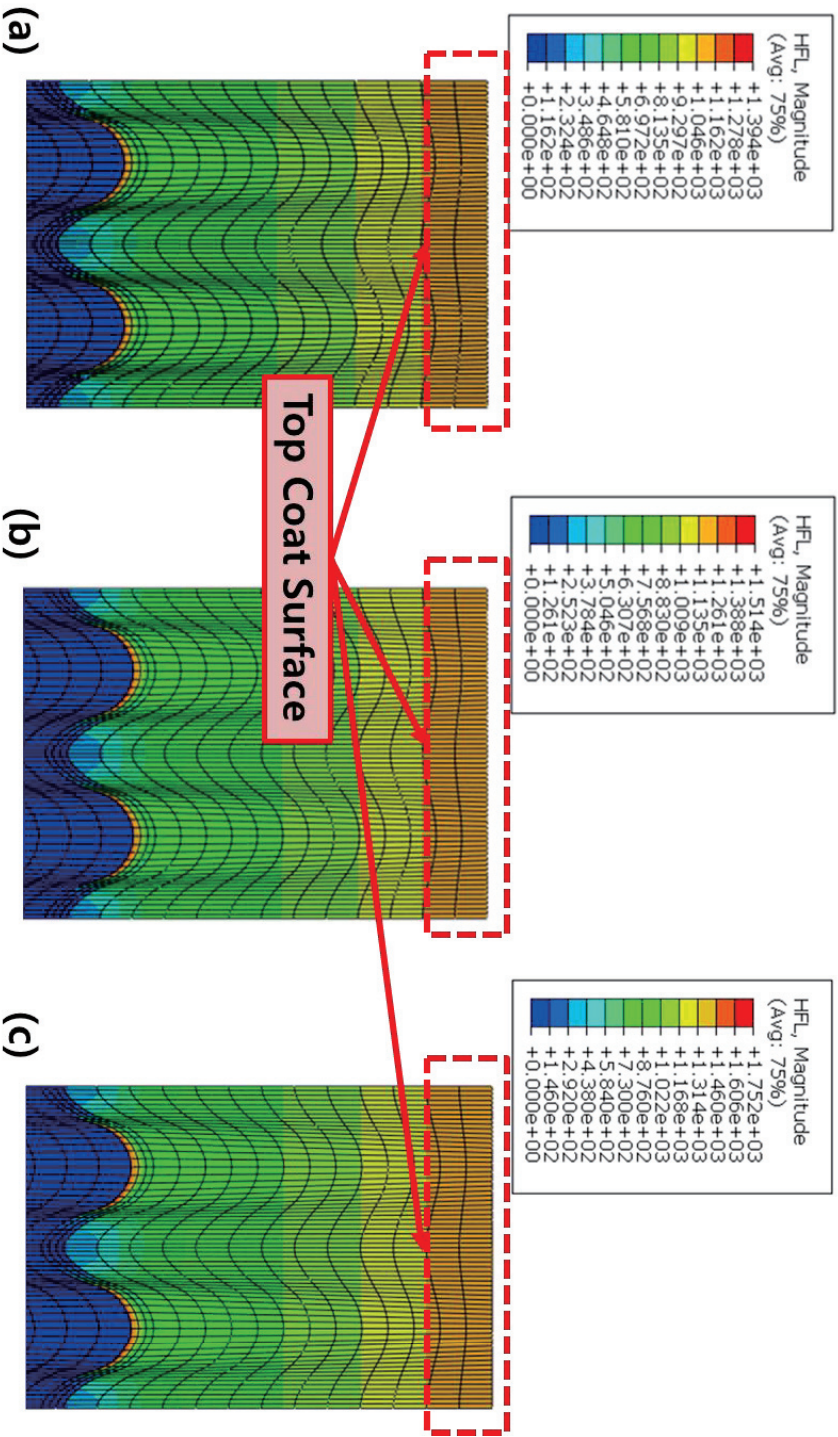


Figure 15. Heat transfer analysis at (a) 900°C; (b) 1000°C; (c) 1200°C

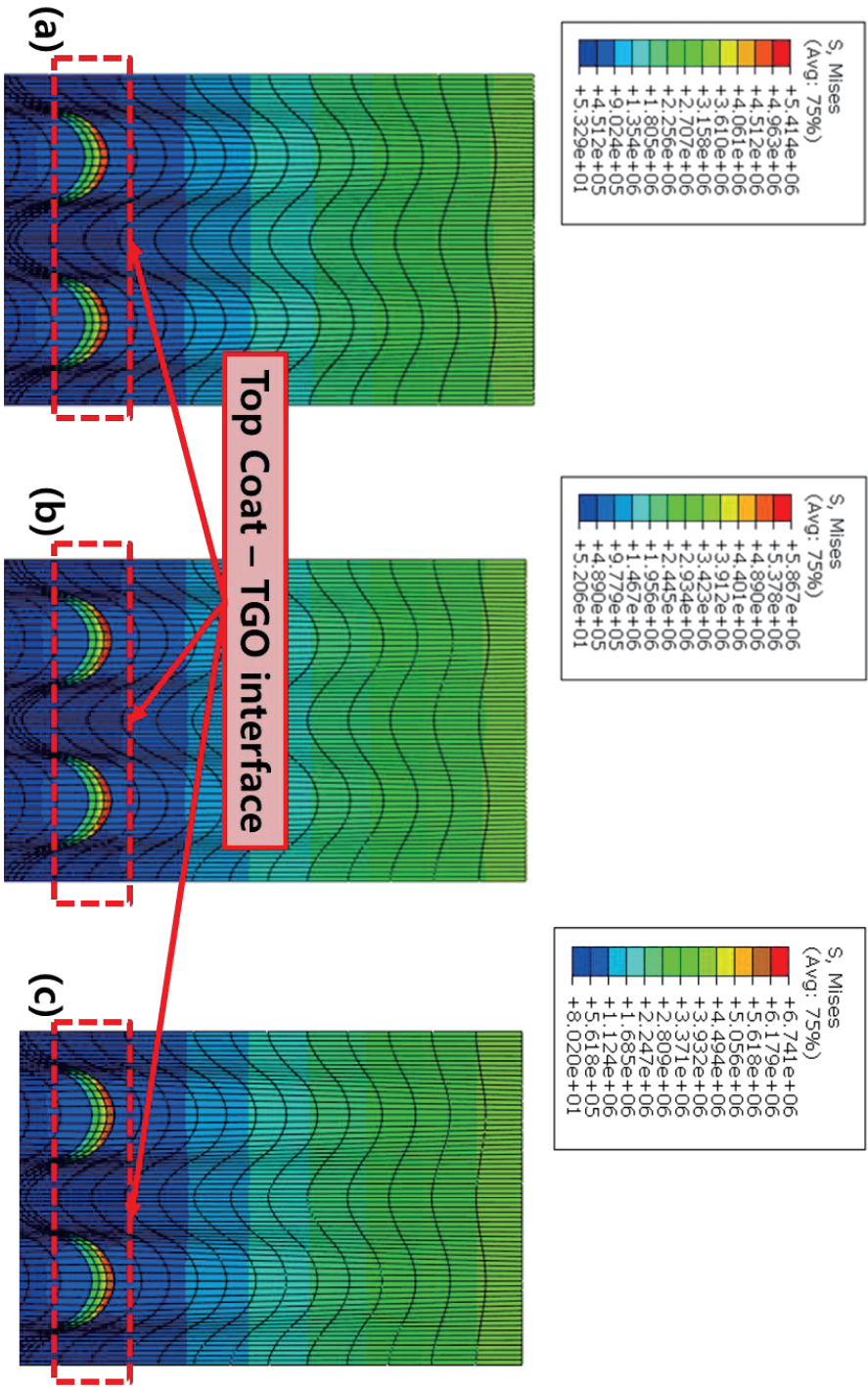


Figure 16. Thermal loading analysis at (a) 900°C; (b) 1000°C; (c) 1200°C

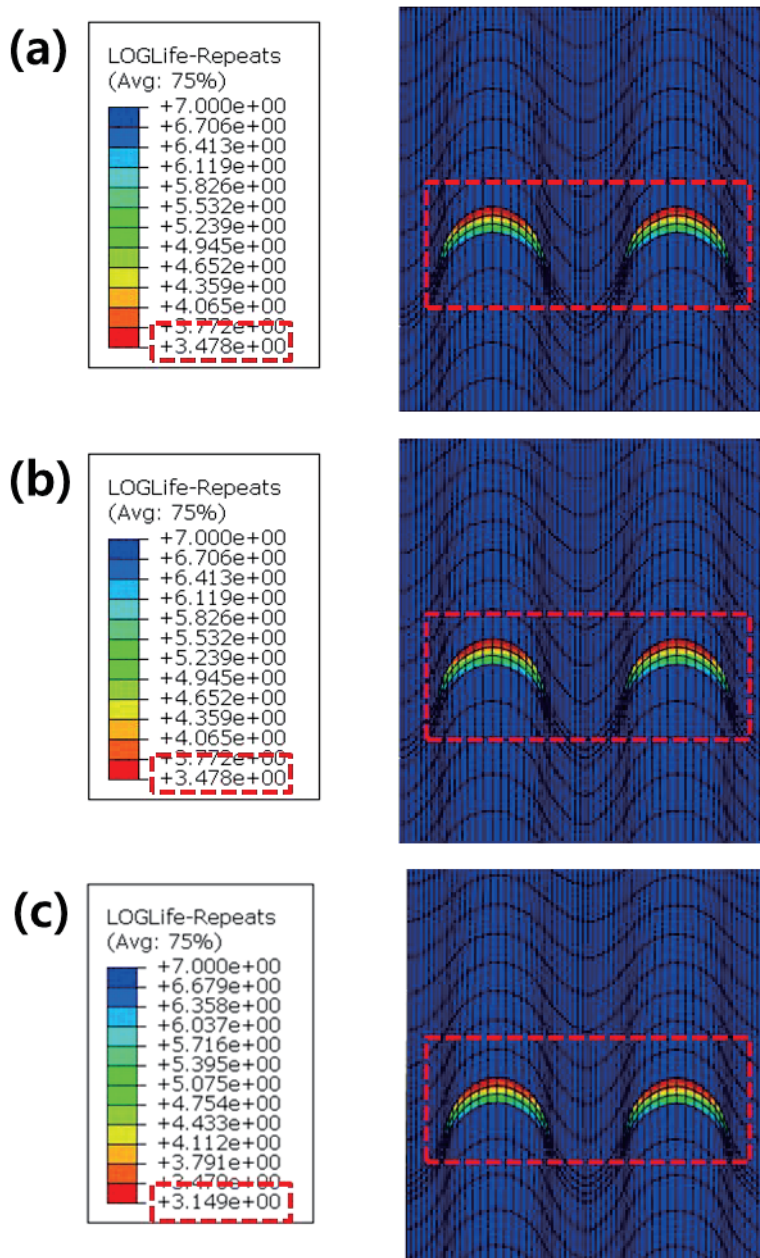


Figure 17. Crack initiation cycle analysis at (a) 900°C; (b) 1000°C; (c) 1200°C

Table 10. Crack initiation cycle for various thermal loading

Temperature	Log life	Actual life
900°C	3.657	4539.42 cycles
1000°C	3.478	3006.08 cycles
1100°C	3.285	1927.52 cycles
1200°C	3.149	1409.29 cycles

Table 11. Crack propagation cycle for various thermal loading

Temperature	Life
900°C	1286 cycles
1000°C	927 cycles
1100°C	783 cycles
1200°C	623 cycles

Table 12. Final fracture cycle for various thermal loading

Temperature	Crack initiation life (N_i)	Crack propagation life (N_p)	Total Life (N_f)
900°C	4539.42 cycles	1286 cycles	5825.42 cycles
1000°C	3006.08 cycles	927 cycles	3933.08 cycles
1100°C	1927.52 cycles	783 cycles	2710.52 cycles
1200°C	1409.29 cycles	623 cycles	2032.29 cycles

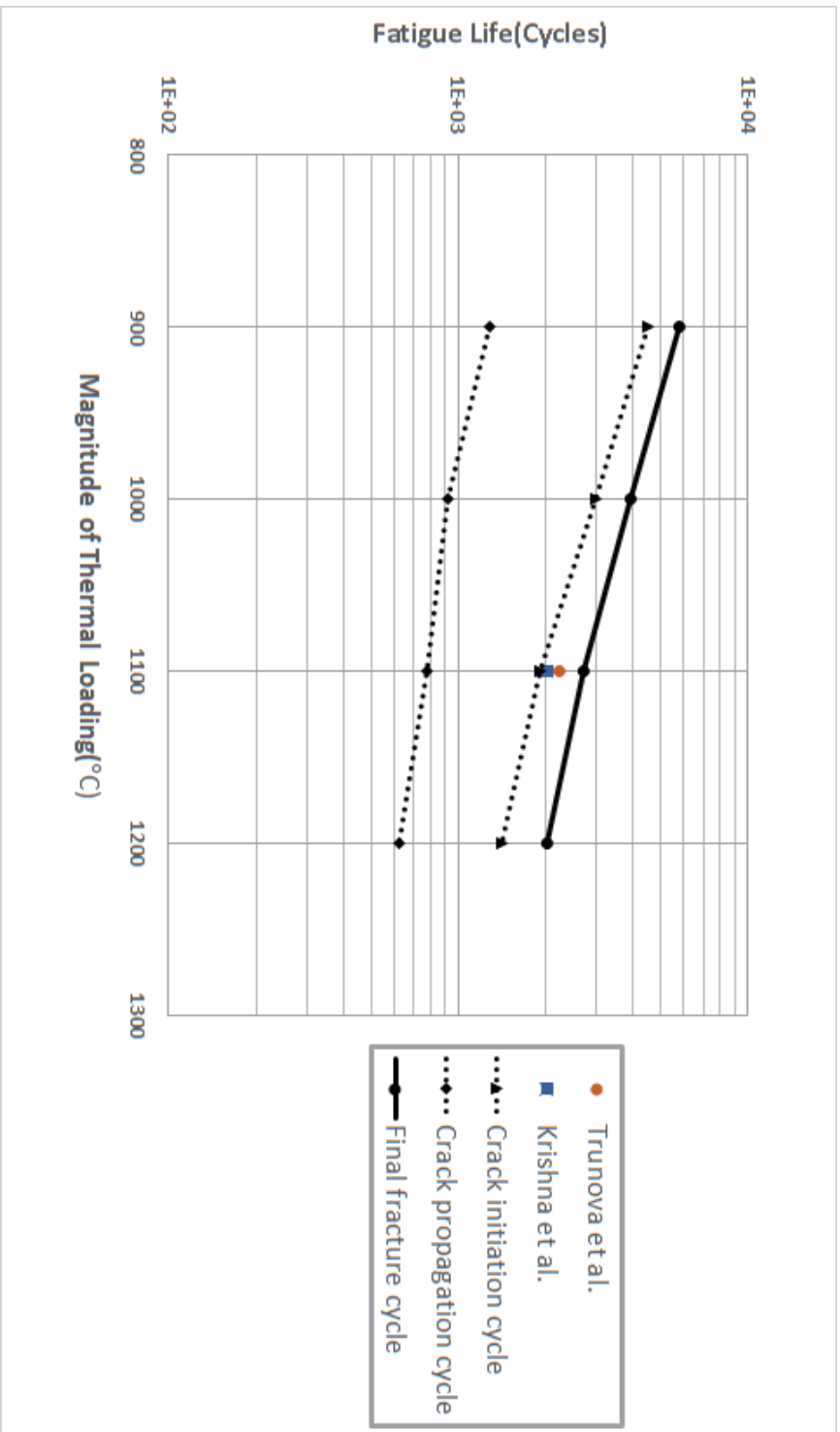


Figure 18. Fatigue life for various thermal loading

5. Conclusion and future works

5.1. Conclusion

Based on the strain–life relation and fracture mechanics, we predicted the fatigue life for the thermal barrier coating and compared the results with the experimental results. And with this results, we also examined the effect of high temperature on the structure. The local approach using the strain–life relation predicted the crack initiation position and the number of cycles, and calculated the number of cycles from crack initiation to final failure considering crack growth based on fracture mechanics. Despite the classical model, the paris' law, which only considers region II , predicts the cycle at the propagation stage quite well.

The simulation process was largely divided into two parts, and the validity of the simulation was verified by comparing with the experimental results. The experimental environment, such as cooling time, internal defects, and types of materials, could not be perfectly matched. An additional analysis was conducted to see fatigue life for

various thermal loadings. As the size of thermal loading increased, the lifespan tended to decrease. Additionally magnitude of thermal loading increases, the number of changes in fracture cycles tends to decrease. This proved to require a slightly more delicate design for TBCs used at various temperatures.

5.2. Future works

In this thesis, the starting point of the crack was found directly through the local approach. Also, to get J–integral value, we define crack manually along crack path. Therefore, the proposed study has the limitation that it is possible to predict crack propagation only if the location of crack is defined. For more accurate prediction of fatigue life, a simulation technique should be devised to predict crack initiation spot and crack propagation path at once.

Internal defects in materials such as micro cracks were also not considered. In the case of normal material failure, there are many cases where the crack starts from existing internal defects and reaches final failure, not external impact. The material with actual

internal defects may have a shorter life than expected and conservative application is required. Therefore, for reliable results, a method that can take into account the structure of the micro scale should be devised.

6. Reference

- [1] M. Jinnestrand and H. Brodin, "Crack initiation and propagation in air plasma sprayed thermal barrier coatings, testing and mathematical modelling of low cycle fatigue behaviour," *Materials Science and Engineering: A*, vol. 379, no. 1-2, pp. 45-57, 2004.
- [2] K. Obrtlík, S. Hutařová, L. Čelko, M. Juliš, T. Podrábský, and I. Šulák, "Effect of Thermal Barrier Coating on Low Cycle Fatigue Behavior of Cast Inconel 713LC at 900 °C," *Advanced Materials Research*, vol. 891-892, pp. 848-853, 2014.
- [3] I.-W. C. Shih-Yu Liu, "Fatigue of Yttria-Stabilized Zirconia: II, Crack Propagation, Fatigue Striations, and Short-Crack Behavior," *Journal of American Ceramic*, vol. 74, pp. 1206-1216, 1991.
- [4] M. Gupta, K. Skogsberg, and P. Nylén, "Influence of Topcoat-Bondcoat Interface Roughness on Stresses and Lifetime in Thermal Barrier Coatings," *Journal of Thermal Spray Technology*, vol. 23, no. 1-2, pp. 170-181, 2013.
- [5] C. Bargraser *et al.*, "Life approximation of thermal barrier coatings via quantitative microstructural analysis," *Materials Science and Engineering: A*, vol. 549, pp. 76-81, 2012.
- [6] K. P. Jonnalagadda *et al.*, "A study of damage evolution in high purity nano TBCs during thermal cycling: A fracture mechanics based modelling approach," *Journal of the European Ceramic Society*, vol. 37, no. 8, pp. 2889-2899, 2017.
- [7] A. M. P. de Jesus, A. L. L. da Silva, and J. A. F. O. Correia, "Fatigue of riveted and bolted joints made of puddle iron-A numerical approach," (in English), *Journal of Constructional Steel Research*, vol. 102, pp.

- 164–177, Nov 2014.
- [8] W. Weibull, *Fatigue Testing and Analysis of Results*. London: Pergamon Press LTD., 1961.
 - [9] Y. L. Lee, J. Pan, R. B. Hathaway, and M. E. Barkey, *Fatigue Testing and Analysis (Theory and Practice)*. Burlington, MA: Elsevier, 2005.
 - [10] E. Castillo, A. Fernandez–Canteli, and A. S. Hadi, "On fitting a fatigue model to data," (in English), *International Journal of Fatigue*, vol. 21, no. 1, pp. 97–106, Jan 1999.
 - [11] E. Castillo and A. Fernandez–Canteli, "A parametric lifetime model for the prediction of high-cycle fatigue based on stress level and amplitude," (in English), *Fatigue & Fracture of Engineering Materials & Structures*, vol. 29, no. 12, pp. 1031–1038, Dec 2006.
 - [12] F. Ellyin, *Fatigue Damage, Crack Growth and Life Prediction*. Springer, 1997.
 - [13] J. D. Morrow, "Cyclic plastic strain energy and fatigue of metals," in *Internal Friction, Damping, and Cyclic Plasticity*, B. Lazan, Ed. West Conshohocken, PA: ASTM International, 1965, pp. 45–87.
 - [14] W. Ramberg and W. R. Osgood, "Description of stress–strain curves by three parameters," National Advisory Committee for Aeronautics, Washington, DC. Technical Report No. 992, 1943.
 - [15] E. Castillo and A. Fernandez–Canteli, "A general regression model for lifetime evaluation and prediction," (in English), *International Journal of Fracture*, vol. 107, no. 2, pp. 117–137, Jan 2001.
 - [16] N. Patil, P. Mahadevan, and A. Chatterjee, "A constructive empirical theory for metal fatigue under block cyclic loading," (in English), *Proceedings of the Royal Society a-Mathematical Physical and Engineering Sciences*, vol. 464, no. 2093, pp. 1161–1179, May 8 2008.
 - [17] J. P. Cusumano and A. Chatterjee, "Steps towards a qualitative

- dynamics of damage evolution," (in English), *International Journal of Solids and Structures*, vol. 37, no. 44, pp. 6397–6417, Nov 2000.
- [18] E. Castillo, A. Fernandez–Canteli, H. Pinto, and M. L. Ruiz–Ripoll, "A statistical model for crack growth based on tension and compression Wohler fields," (in English), *Engineering Fracture Mechanics*, vol. 75, no. 15, pp. 4439–4449, Oct 2008.
- [19] H. Tada, P. C. Paris, and G. R. Irwin, *The stress analysis of cracks handbook*, 3rd edition ed. New York: ASME Press, 2000.
- [20] A. Carpinteri and A. Spagnoli, "A fractal analysis of size effect on fatigue crack growth," (in English), *International Journal of Fatigue*, vol. 26, no. 2, pp. 125–133, Feb 2004.
- [21] A. Spagnoli, "Self–similarity and fractals in the Paris range of fatigue crack growth," (in English), *Mechanics of Materials*, vol. 37, no. 5, pp. 519–529, May 2005.
- [22] R. O. Ritchie, "Incomplete self–similarity and fatigue–crack growth," (in English), *International Journal of Fracture*, vol. 132, no. 3, pp. 197–203, Apr 2005.
- [23] N. Pugno, M. Ciavarella, P. Cornetti, and A. Carpinteri, "A generalized Paris' law for fatigue crack growth," (in English), *Journal of the Mechanics and Physics of Solids*, vol. 54, no. 7, pp. 1333–1349, Jul 2006.
- [24] P. Paris and F. Erdogan, "A critical analysis of crack propagation laws," *Journal of Basic Engineering*, vol. 85, no. 4, pp. 528–534, 1960.
- [25] R. G. Forman, V. E. Kearney, and R. M. Engle, "Numerical Analysis of Crack Propagation in Cyclic–Loaded Structures," (in English), *Journal of Basic Engineering*, vol. 89, no. 3, pp. 459–&, 1967.
- [26] F. Erdogan and M. Ratwani, "Fatigue and Fracture of Cylindrical Shells Containing a Circumferential Crack," (in English), *International Journal*

- of Fracture Mechanics*, vol. 6, no. 4, pp. 379–392, 1970.
- [27] R. G. Forman and S. R. Mettu, "Behavior of surface and corner cracks subjected to tensile and bending loads in ti 6al-4v alloy," in *Fracture mechanics: twenty-second symposium*, Philadelphia, 1992, vol. vol 1. American Society for Testing and Materials, pp. 519–546.
- [28] NASGRO, "Fatigue crack growth computer program NASGRO Version 3.0-reference manual," ed, 2000.
- [29] H. Y. Agha, A. S. Beranger, R. Billardon, and F. Hild, "High-cycle fatigue behaviour of spheroidal graphite cast iron," (in English), *Fatigue & Fracture of Engineering Materials & Structures*, vol. 21, no. 3, pp. 287–296, Mar 1998.
- [30] I. Chantier, V. Bobet, R. Billardon, and F. Hild, "A probabilistic approach to predict the very high-cycle fatigue behaviour of spheroidal graphite cast iron structures," (in English), *Fatigue & Fracture of Engineering Materials & Structures*, vol. 23, no. 2, pp. 173–180, Feb 2000.
- [31] E. Castillo, A. Fernandez-Canteli, and D. Siegele, "Obtaining S-N curves from crack growth curves: an alternative to self-similarity," (in English), *International Journal of Fracture*, vol. 187, no. 1, pp. 159–172, May 2014.
- [32] R. A. Miller, "Oxidation-Based Model for Thermal Barrier Coating Life," *Journal of the American Ceramic Society*, vol. 67, no. 8, pp. 517–521, 1984.
- [33] C. Ping-wei, W. Shao-ming, and W. Feng-Hui, "Fracture Analysis of Thermal Barrier Coating Delamination under Thermal Shock," *Procedia Engineering*, vol. 99, pp. 344–348, 2015.
- [34] M. Bäker and P. Seiler, "A Guide to Finite Element Simulations of Thermal Barrier Coatings," *Journal of Thermal Spray Technology*, vol.

- 26, no. 6, pp. 1146–1160, 2017.
- [35] G. Fajdiga and M. Sraml, "Fatigue crack initiation and propagation under cyclic contact loading," *Engineering Fracture Mechanics*, vol. 76, no. 9, pp. 1320–1335, 2009.
- [36] R. Krueger, "Virtual crack closure technique: history, approach, and applications," *Applied Mechanics Reviews*, vol. 57, no. 2, pp. 109–143, 2004.
- [37] R. F. Sanches, A. M. P. de Jesus, J. A. F. O. Correia, A. L. L. da Silva, and A. A. Fernandes, "A probabilistic fatigue approach for riveted joints using Monte Carlo simulation," (in English), *Journal of Constructional Steel Research*, vol. 110, pp. 149–162, Jul 2015.
- [38] T. Svensson, "Mean Value Influence in Fatigue – on the rational choice of model complexity," *International Journal of Fatigue*, 2003.
- [39] N. E. Dowling, "Mean stress effects in strain–life fatigue," *Fatigue & Fracture of Engineering Materials & Structures*, vol. 32, no. 12, pp. 1004–1019, 2009.
- [40] A. H. Noroozi, G. Glinka, and S. Lambert, "A two parameter driving force for fatigue crack growth analysis," (in English), *International Journal of Fatigue*, vol. 27, no. 10–12, pp. 1277–1296, Oct–Dec 2005.
- [41] *The Effect of Stress Ratio During Crack Propagation and fatigue for 2024–T3 and 7075–T6 Aluminum*, 1970.
- [42] J. Maierhofer, R. Pippan, and H. P. Ganser, "Modified NASGRO equation for physically short cracks," (in English), *International Journal of Fatigue*, vol. 59, pp. 200–207, Feb 2014.
- [43] NASA–JSC, *NASGRO® Fracture Mechanics and Fatigue Crack Growth Analysis Software*. NASA–JSC and Southwest Research Institute, 2006.
- [44] F. R.G. and M. S.R., "Behavior of surface and corner cracks subjected

- to tensile and bending loads in Ti-6Al-4V alloy," in *Fracture Mechanics: 22nd Symposium*, Philadelphia, 1992: ASTM STP 1131, American Society for Testing and Materials.
- [45] J. C. Newman, "A Crack Opening Stress Equation for Fatigue Crack-Growth," (in English), *International Journal of Fracture*, vol. 24, no. 4, pp. R131-R135, 1984.
- [46] R. G. Forman, "Study of fatigue crack initiation from flaws using fracture mechanics theory," *Engineering Fracture Mechanics*, vol. 4, no. 2, pp. 333-345, 1972.
- [47] A. Hartman and A. Schijve, "The effects of environment and load frequency on the crack propagation law for macro fatigue crack growth in aluminium alloys," *Engineering Fracture Mechanics*, vol. 1, no. 4, pp. 615-631, 1970.
- [48] J. J. Kruzic and R. O. Ritchie, "Kitagawa-Takahashi diagrams define the limiting conditions for cyclic fatigue failure in human dentin," (in English), *Journal of Biomedical Materials Research Part A*, vol. 79a, no. 3, pp. 747-751, Dec 1 2006.
- [49] S. Kyaw, A. Jones, M. A. E. Jepson, T. Hyde, and R. C. Thomson, "Effects of three-dimensional coating interfaces on thermo-mechanical stresses within plasma spray thermal barrier coatings," *Materials & Design*, vol. 125, pp. 189-204, 2017.
- [50] I.-H. Shin, J.-M. Koo, C.-S. Seok, S.-H. Yang, T.-W. Lee, and B.-S. Kim, "Estimation of spallation life of thermal barrier coating of gas turbine blade by thermal fatigue test," *Surface and Coatings Technology*, vol. 205, pp. S157-S160, 2011.
- [51] J. Song, S. Li, X. Yang, H. Qi, and D. Shi, "Numerical investigation on the cracking behaviors of thermal barrier coating system under different thermal cycle loading waveforms," *Surface and Coatings*

Technology, vol. 349, pp. 166–176, 2018.

- [52] O. Trunova, T. Beck, R. Herzog, R. W. Steinbrech, and L. Singheiser, "Damage mechanisms and lifetime behavior of plasma sprayed thermal barrier coating systems for gas turbines—Part I: Experiments," *Surface and Coatings Technology*, vol. 202, no. 20, pp. 5027–5032, 2008.
- [53] K. P. Jonnalagadda, R. Eriksson, X.-H. Li, and R. L. Peng, "Fatigue life prediction of thermal barrier coatings using a simplified crack growth model," *Journal of the European Ceramic Society*, vol. 39, no. 5, pp. 1869–1876, 2019.

국문초록

변형률-수명 관계와 균열 성장 모델을 고려한 열차폐 코팅의 피로수명 예측

김 연 준

기계항공공학부

서울대학교 대학원

터빈 블레이드와 같은 열 구조에서 열 차단 코팅 (TBC)의 역할은 매우 중요하다. TBC는 극한의 가스 온도로부터 재료를 보호하는 역할을 하기 때문에 TBC의 고장은 구조물의 기능에 직접적인 영향을 미친다. 따라서 TBC의 주기적 열 하중으로 인한 피로 수명 예측은 중요하게 연구되어야 한다. 본 논문에서는 상용 소프트웨어 인 ABAQUS를 사용하여 TBC의 피로 수명을 조사했다. 재료 파괴에 대한 일반적인 메커니즘은 균열의 시작, 전파 및 최종 파단을 따른다. 따라서 TBC의 피로 수명은 균열 시작주기와 균열 전파주기의 합으로 예측한다. 예측을 위해 Paris가 제안한 균열 성장 모델과 Morrow 변형 수명 관계가 사용되었다. ABAQUS내에서 계산의 정확도를 높이기 위해 contour

integral method를 사용하여 J-integral 값을 얻어냈다. 또한 ABAQUS-Python script와 MATLAB을 통해 후처리 및 수치적분 과정을 진행하여 피로수명을 계산해냈다. 시뮬레이션 결과를 검증하기 위해, 참고문헌으로부터 얻은 실험결과와 비교하였으며, 오차범위 내에서 어느 정도 일치하는 것을 확인할 수 있었다. 또한 추가적인 해석을 통해 다양한 열 하중에 대한 피로수명에 대한 경향성을 볼 수 있었다. 온도가 올라갈수록 fatigue life가 감소하고, 감소폭 역시 점점 작아지는 경향성을 볼 수 있었다.

Keywords : 피로파괴 해석, 열 차단 코팅, 피로 수명 예측, 균열 시작, 균열 전파, 파괴 역학, 열 주기적 하중 피로

Student Number : 2018-27842